AGU PUBLICATIONS

Water Resources Research

RESEARCH ARTICLE

10.1002/2016WR018907

Key Points:
- Solute transport in vegetated aquatic flows
- Development of a computationally efficient semianalytical solution for the concentration
- Vegetation permeability has a key role in regulating transport

Correspondence to:
F. P. J. de Barros,
fbarros@usc.edu

Citation:
Rubol, S., I. Battiato, and F. P. J. de Barros (2016), Vertical dispersion in vegetated shear flows, *Water Resour. Res.*, *52*, doi:10.1002/2016WR018907.

Received 7 MAR 2016
Accepted 19 SEP 2016
Accepted article online 26 SEP 2016

Vertical dispersion in vegetated shear flows

Simonetta Rubol[1], Ilenia Battiato[2], and Felipe P. J. de Barros[3]

[1]Department of Biological Sciences, University of Southern California, Los Angeles, California, USA, [2]Energy Resources Engineering, Stanford University, Stanford, California, USA, [3]Sonny Astani Department of Civil and Environmental Engineering, University of Southern California, Los Angeles, California, USA

Abstract Canopy layers control momentum and solute transport to and from the overlying water surface layer. These transfer mechanisms strongly dependent on canopy geometry, affect the amount of solute in the river, the hydrological retention and availability of dissolved solutes to organisms located in the vegetated layers, and are critical to improve water quality. In this work, we consider steady state transport in a vegetated channel under fully developed flow conditions. Under the hypothesis that the canopy layer can be described as an effective porous medium with prescribed properties, i.e., porosity and permeability, we model solute transport above and within the vegetated layer with an advection-dispersion equation with a spatially variable dispersion coefficient (diffusivity). By means of the *Generalized Integral Transform Technique*, we derive a semianalytical solution for the concentration field in submerged vegetated aquatic systems. We show that canopy layer's permeability affects the asymmetry of the concentration profile, the effective vertical spreading behavior, and the magnitude of the peak concentration. Due to its analytical features, the model has a low computational cost. The proposed solution successfully reproduces previously published experimental data.

1. Introduction

Vegetation exerts a major role in regulating water quality and riverbanks stability by increasing bed roughness and decreasing near-bed turbulent stress. Canopies create an additional drag that decreases the flow velocity within the vegetated layer. This velocity reduction shelters biota and promotes the hydrological storage and retention of nutrients, heavy metals, and microbes, as well as the trapping of sediments inside the canopy layer [e.g., *Costanza et al.*, 1997; *Nepf*, 2012]. Canopy layers behave as a mass-transfer limited system that exchanges mass and momentum with the overlying water surface layer [*Ghisalberti and Nepf*, 2005; *Lowe et al.*, 2005; *Variano et al.*, 2009]. These transfer mechanisms, strongly dependent on canopy geometry, affect the amount of solute in the river as well as the hydrological retention and availability of dissolved solutes to organisms located in the vegetated layers. One such example, relevant to processes in the hyporheic zone, includes the mass transfer to sediments microflora [*Thomas et al.*, 2000]. These effects are particularly relevant in dense canopies, where the vegetation drag is sufficient to induce an inflection point in the mean velocity profile at the top of the vegetation [e.g., *Ghisalberti and Nepf*, 2002; *Konings et al.*, 2012; *Luhar et al.*, 2008]. As a result, the turbulent stress penetrates the canopy layer only partially leading to the formation of high- and low-exchange zones in the upper part of the canopies and close to the river bed, respectively [*Ghisalberti and Nepf*, 2005].

Given canopies' crucial role in regulating eco-services and water management, transport in vegetated systems needs to be quantified in order to predict solute distribution and peak concentrations due to chemical releases in rivers. The latter is directly linked to the magnitude of both environmental and human health risks which are, in turn, affected by the density of the canopy. Additionally, transport models can provide insights for designing experimental apparati and predict the effect of vegetation on river metabolism (e.g., the Biological Oxygen Demand).

In vegetated aquatic environments, the free flow layer is responsible for transporting solutes faster while the canopy layer tends to retain the chemical substances. The importance of vertical velocity profiles on solute breakthrough is a well-studied subject in hydrology and the environmental fluid mechanics communities [e.g., *Fischer*, 1979]. The interplay between shear flow and mixing in vegetated aquatic systems has been investigated in the literature [e.g., *Ghisalberti and Nepf*, 2005; *Poggi et al*., 2009; *Nepf*, 2012]. Strategies for quantifying transport in vegetated rivers consist of lumped-parameter models [*Ghisalberti and Nepf*, 2005], upscaled models [*Marion et al*., 2008], and numerical solution of the advection-dispersion equation [*Kang and Choi*, 2009]. The fast time scale associated with open surface flows requires the need to develop computationally fast solutions that capture the main physical attributes of the system. This is particularly important for contamination originating from accidental spills or extreme events where real-time solutions are needed to provide the basis of rational decision making and clean up strategy. Within this context, and with the aim of alleviating the associated computational burden associated with numerical methods, we propose the use of a reduced-complexity semiempirical model for the velocity field that enables to map the effects of the obstructed shear flow on transport predictions by means of analytical tools.

With the objective of capturing the effects of the velocity profile (induced by the presence of vegetation) on transport predictions, we develop a computationally efficient semianalytical solution for the solute concentration. The solution methodology is based on the well-established *Generalized Integral Transform Technique* [e.g., *Cotta*, 1993; *Sphaier et al*., 2011; *Cotta et al*., 2013] which provides a hybrid analytical-numerical solution for the model prediction. This technique has its origins in the heat transfer and fluid flow community [e.g., *Cotta*, 1993; *Özişik and Mikhailov*, 1994] and has been used to address pollutant dispersion in channels in the absence of canopies [*de Barros et al*., 2006; *de Barros and Cotta*, 2007]. The works of *de Barros et al*. [2006] and *de Barros and Cotta* [2007] derived solutions for the advection-dispersion equation with spatially variable coefficients in two- and three-dimensions. *Guerrero and Skaggs* [2010] adopted the integral transform method of *Cotta* [1993] to develop a solution for the one-dimensional advection-dispersion equation with distance-dependent coefficients. *Hirata et al*. [2009] used the same methodology to investigate the stability of natural heat convection in a fluid layer overlying a homogeneous porous medium. In this work, we apply it for the first time to investigate the impact of vegetation on solute transport. The methodology is appealing since it is flexible and computationally inexpensive in comparison to existing numerical models. The velocity profile we adopt is based on the two-domain model proposed by *Battiato and Rubol* [2014]. The proposed flow model treats the canopy layer as a porous medium [see *Lowe et al*., 2008; *Papke and Battiato*, 2013; *Battiato and Rubol*, 2014] and is coupled to the advection-dispersion equation with spatially variable coefficients. Our work aims to address the following fundamental question: How does vegetation regulate solute dispersion? Our results show that the asymmetry of the solute concentration profile, and therefore the peak concentration and overall dispersive behavior are mainly controlled by the geometrical properties of the canopy. Finally, the predictive capabilities of the model are successfully tested using the experimental tracer data of *Ghisalberti and Nepf* [2005].

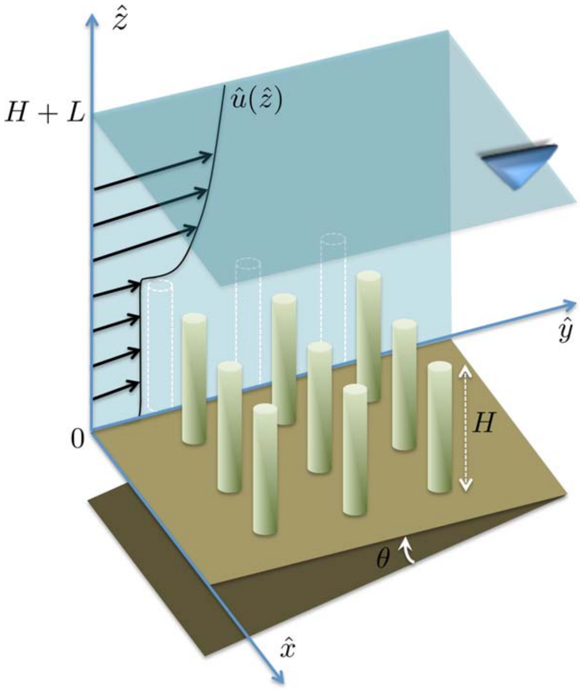

Figure 1. Schematic illustration of the flow domain under consideration. Adapted from *Battiato and Rubol* [2014].

The paper is structured as follows: section 2 describes the flow model of *Battiato and Rubol* [2014]. The transport formulation and the solution methodology are given in section 3. Results are analyzed in section 4. Conclusions are provided in section 5.

2. Turbulent Flow Over a Permeable Layer

We consider a 2-D fully developed incompressible turbulent flow in an open channel of total height $H+L$ and slope $\theta \ll 1$ with $S_0 := \tan\theta \approx \theta$ (such that $S_0 \approx \sin\theta$), whose bottom part, $\hat{z} \in (0, H)$, is occupied by an undeformable porous medium of permeability

K constituted of a regular array of rigid cylinders transverse to the mean flow (see Figure 1). Such an obstruction model provides a good approximation of rigid, or moderately flexible, submerged aquatic canopies.

2.1. Two-Domain Approach

Here we use the flow model proposed by *Battiato* [2012] and *Battiato and Rubol* [2014] as the analytical approximation of the mean velocity profile above and within the obstruction. In the following, we provide the flow model description for completeness.

In the surface layer, the steady state Reynolds' equation for fully developed turbulent flow can be used to describe the mean velocity in the direction parallel to the channel bottom, $\hat{u}(\hat{z})$,

$$\mu\frac{\mathrm{d}^2\hat{u}(\hat{z})}{\mathrm{d}\hat{z}^2}-\rho\frac{\mathrm{d}\langle\hat{u}'(\hat{z})\hat{v}'(\hat{z})\rangle}{\mathrm{d}\hat{z}}+\rho g S_0=0,\quad \hat{z}\in(H,H+L), \tag{1}$$

where g, μ, and ρ are the gravitational acceleration, the fluid dynamic viscosity and density, respectively. In (1), $\hat{u}'$ and $\hat{v}'$ represent the velocity fluctuations about their respective mean, and $\langle\hat{u}'\hat{v}'\rangle$ is the Reynolds stress. Under a turbulent viscosity hypothesis, i.e., $\langle\hat{u}'\hat{v}'\rangle=-\nu_t(\hat{z})\mathrm{d}_{\hat{z}}\hat{u}$, where ν_t is the eddy viscosity [e.g., *Ghisalberti and Nepf*, 2004; *Poggi et al.*, 2009], the total shear stress $\hat{\tau}(\hat{z})$ can be written as follows:

$$\hat{\tau}(\hat{z}):=\mu\frac{\mathrm{d}\hat{u}(\hat{z})}{\mathrm{d}\hat{z}}-\rho\langle\hat{u}'(\hat{z})\hat{v}'(\hat{z})\rangle=\mu_T(\hat{z})\frac{\mathrm{d}\hat{u}(\hat{z})}{\mathrm{d}\hat{z}},\quad \hat{z}\in(H,H+L), \tag{2}$$

where $\mu_T:=\mu+\rho\nu_t(\hat{z})$.

Turbulent flows above canopy layers can be also described with any of the empirically available variants of the *log law* [*Stephan and Gutknecht*, 2002], e.g.,

$$\hat{u}(\hat{z})=\hat{U}+\frac{\hat{u}_\tau}{\kappa}\ln\left(\frac{\hat{z}}{H}\right),\quad \hat{z}\in(H,H+L), \tag{3}$$

where $\kappa=0.19$ is the reduced von Kármán constant [*Kubrak et al.*, 2008], $\hat{U}$ is the (mean) velocity at the top of the canopies, and $\hat{u}_\tau$ is the friction velocity defined in terms of the stress at the interface between the free and filtration flows, $\hat{\tau}(H^+)$:

$$\hat{u}_\tau:=\sqrt{\frac{\hat{\tau}(H^+)}{\rho}}. \tag{4}$$

Equation (3) prescribes that the mean velocity profile approaching the canopies from above ($\hat{z}\to H^+$) should (i) match the mean interfacial velocity $\hat{U}$ between the free and filtration flows and (ii) follow a translated log profile away from the free surface ($\hat{z}<H+L$).

Inside the canopies, the Darcy-Brinkman equation is customarily employed to describe the horizontal component of the intrinsic mean velocity $\hat{u}(\hat{z})$ [e.g., *Stephan and Gutknecht*, 2002; *Katul et al.*, 2011],

$$\mu_e\frac{\mathrm{d}^2\hat{u}(\hat{z})}{\mathrm{d}\hat{z}^2}-\frac{\mu_e}{K}\hat{u}(\hat{z})+\rho g S_0=0,\quad \hat{z}\in(0,H), \tag{5}$$

where K [L^2] is the canopy permeability and μ_e is the fluid "effective" viscosity, respectively. Since experimental evidence suggests smoothness of the mean velocity profile at the interface, we set $\mu_e:=\mu_T(H^+)$ in (5) [*Katul et al.*, 2011; *Papke and Battiato*, 2013]. An estimate of $\mu_T(H^+)$ can be readily determined through a consistency argument applied to (3) and (1). Integrating (1) from $\hat{z}=H$ to $\hat{z}=H+L$, while accounting for (2) and the zero shear condition at the free surface, $\hat{\tau}(H+L)=0$, yields

$$\hat{\tau}(H^+)=\rho g S_0 L\quad\text{and}\quad \hat{u}_\tau=\sqrt{gS_0L}. \tag{6}$$

Consistency between the *log law* (3) where $\hat{u}_\tau$ is given by (6), and the turbulent viscosity hypothesis (2) requires that $\mu_T(H^+)\mathrm{d}_{\hat{z}}\hat{u}|_{H^+}=\rho g S_0 L$, where $\hat{u}$ is defined by (3). This yields to a self-consistent estimate of μ_T at the interface between the free and vegetated flows [*Battiato and Rubol*, 2014].

$$\mu_T(H^+)=\rho\kappa H\hat{u}_\tau. \tag{7}$$

As experimental evidence suggests [e.g., *Ghisalberti and Nepf*, 2004; *White and Nepf*, 2007; *Poggi et al.*, 2009], equations (3) and (5) are subject to no shear condition at $\hat{z}=0$, i.e., $\hat{\tau}(0)=0$, and continuity of velocity and shear stress at the interface between the free and filtration flows $\hat{z}=H$, i.e., $\hat{u}(H^-)=\hat{u}(H^+)=\hat{U}$ and $\mu_e \mathrm{d}_{\hat{z}}\hat{u}|_{H^-}=\mu_T(H^+)\mathrm{d}_{\hat{z}}\hat{u}|_{H^+}$.

2.2. Analytical Solution for the Flow Field

Choosing the height of the canopies H, the effective viscosity μ_e, and the velocity scale $q=\rho g S_0 H^2/\mu_e$ as repeating variables, we rescale lengths and velocities by H and q, respectively, and define the following dimensionless quantities:

$$z=\frac{\hat{z}}{H},\quad u=\frac{\hat{u}}{q},\quad \delta=\frac{L}{H},\quad U=\frac{\hat{U}}{q},\quad \lambda^2=\frac{H^2}{K}, \tag{8}$$

where δ is the dimensionless channel depth and λ is the inverse of the dimensionless permeability. Notice that denser canopy corresponds to lower K or, equivalently, higher values of λ. The analytical solution of (5) and (3) for the dimensionless mean velocity profile $u(z)$ inside and above the canopy layer is [*Battiato and Rubol*, 2014]

$$u(z)=\lambda^{-2}+C(e^{\lambda z}+e^{-\lambda z}),\quad z\in(0,1], \tag{9a}$$

$$u(z)=U+\delta\ln z,\quad z\in(1,1+\delta), \tag{9b}$$

respectively, with

$$C=\frac{1}{2}\delta\lambda^{-1}\mathrm{csch}\lambda, \tag{10a}$$

$$U=\lambda^{-2}+\delta\lambda^{-1}\coth\lambda, \tag{10b}$$

and $U:=u(1)$ denoting the interfacial velocity.

The model is amenable of analytical solution for the mean velocity, and allows one to determine closed-form expressions for a number of relevant physical quantities, including volumetric discharge, bulk velocity, penetration length, drag length scale, and canopy shear layer parameter (CSL), without relying on additional parametrization. All such quantities can be uniquely quantified from the channel geometrical features, once the canopy layer permeability has been estimated (e.g., from canopy density). However, the applicability of the flow model in its current form is limited to steady state fully developed flows above and between rigid (or moderately flexible) and spatially homogenous canopy layers. Generalizations to flexible and spatially heterogeneous canopies would require (i) a coupling between the mechanics of the canopy bending and the hydrodynamics and (ii) solution of equation (5) with nonconstant coefficients, i.e., $K(\hat{z})$. The solution accurately describes experimental (mean) velocity profiles both inside and above the obstruction, except in proximity of the free interface were the *log law* is invalid [*Battiato and Rubol*, 2014]. Noticeably, (9) contains only one model parameter, namely the dimensionless permeability λ. The latter can be estimated from canopy density as described in *Battiato and Rubol* [2014] and allows one to directly correlate obstruction morphology (e.g., LAI, porosity, canopy height) to the dynamic response of flow and transport in and above arrays of rigid cylinders. Yet, the derivation of a formal expression that links canopy density to the permeability of natural vegetation is current object of investigation. In the following, we employ the analytical solution (9) to study the transport of a passive tracer in a coupled free/filtration flows system.

3. Mass Transport Above a Permeable Layer

We consider the continuous injection of a passive solute released at the inlet of a semi-infinite vegetated channel. Similarly to the approaches available to model momentum transfer, mass transfer in coupled free and filtration flows can be described using either single-domain or multiple-domain approaches. The former employ a single balance equation with spatially varying coefficients to account for different transport mechanisms throughout the domain (e.g., turbulent versus hydrodynamic dispersion in the free and obstructed flows, respectively). The fundamental hypothesis underlying single-domain approaches is that the governing equations in each region should have a similar structure, e.g., that of an advection-dispersion equation (ADE). Instead, multidomain approaches use two different mathematical models (often with constant coefficients in each subdomain), and couple the two formulations through continuity of state variables and their fluxes at the interface. The advantage of multidomain approaches over single-domain models, as apparent in section 2, is that equations with constant coefficients are generally easier to handle analytically. Yet, in section 3.1, we present a single-domain approach for which a semianalytical solution can be found (section 3.2). In section 4 we present a comparison between model predictions and experimental data and show that the model simplifying assumptions are accurate enough for our modeling purposes.

3.1. Single-Domain Approach

Under the assumption that scales are well separated [e.g. *Battiato et al.*, 2009; *Battiato and Tartakovsky*, 2011; *Boso and Battiato*, 2013; *Arunachalam et al.*, 2015; *Ling et al.*, 2016, and references therein], the space-time upscaling of microscale (substem scale) transport leads to a macrodispersion equation for Fickian transport [*White and Nepf*, 2003; *Tanino and Nepf*, 2008; *Nepf and Ghisalberti*, 2008], i.e., under a gradient-diffusion hypothesis and for observation (macroscopic) times greater than turbulent timescales, the mass transport of a passive tracer through and above a canopy layer can be described by the advection-dispersion equation for the space-time averaged concentration $\hat{c}$,

$$\frac{\partial \hat{c}(\hat{y},\hat{z},\hat{t})}{\partial \hat{t}} = \hat{\nabla}\cdot[\hat{\mathbf{D}}(\hat{z})\ \hat{\nabla}\hat{c}(\hat{y},\hat{z},\hat{t}) - \hat{\mathbf{u}}(\hat{z})\hat{c}(\hat{y},\hat{z},\hat{t})], \qquad (\hat{y},\hat{z})\in(0,\infty)\times(0,H+L), \quad \text{and} \quad \hat{t}>0, \tag{11}$$

see *White and Nepf* [2003], *Tanino and Nepf* [2008], and *Nepf* [2012]. In (11), $\hat{\mathbf{u}}$ is a known mean velocity distribution, e.g., (9), and $\hat{\mathbf{D}}$ is the dispersion tensor (or diffusivity), with $[\hat{\mathbf{D}}]_{11}=\hat{D}_\ell$ and $[\hat{\mathbf{D}}]_{22}=\hat{D}_v$, the longitudinal and vertical dispersion coefficients, respectively, and $[\hat{\mathbf{D}}]_{ij}=0$ when $i\neq j$. The total diffusivity $\hat{\mathbf{D}}$ includes both molecular diffusion and the turbulent eddy diffusivity, i.e., the mechanical dispersion due to subscale fluctuations of the velocity field.

Under steady state conditions (i.e., $\partial_t\hat{c}=0$) and for continuous release in a semi-infinite domain, the dispersive mass transfer is mainly vertical since $\partial_{\hat{z}}(\hat{D}_v\partial_{\hat{z}}\hat{c})\sim\hat{D}_v c_o/H^2$, $\partial_{\hat{y}}(\hat{D}_\ell\partial_{\hat{y}}\hat{c})\sim\hat{D}_\ell c_o/Y^2$ with c_o and Y characteristic scales for $\hat{c}$ and the longitudinal spatial direction, respectively, and $H/Y\ll 1$ [see also *Yeh and Tsai*, 1976; *Nokes and Wood*, 1988], i.e., neglecting longitudinal dispersive mass is a justifiable assumption for tracers that are continuously released in time since the main mass-transfer mechanism stems from the vertical dispersive flux [see *McNulty and Wood*, 1984]. Therefore, (11) reduces to

$$u(z)\frac{\partial c(y,z)}{\partial y} = \frac{\partial}{\partial z}\left[D_v(z)\frac{\partial c(y,z)}{\partial z}\right], \quad (y,z)\in(0,\infty)\times(0,1+\delta) \tag{12}$$

where $c(y,z):=\hat{c}/c_o$ is the dimensionless concentration, $D_v=\hat{D}_v/qH$ and $u(z)$ is defined by (9). The concentration at the injection point is denoted by c_o. Equation (12) is subject to

$$\frac{\partial c(y,z)}{\partial z}\Big|_{z=0}=0, \quad \text{and} \quad \frac{\partial c(y,z)}{\partial z}\Big|_{z=1+\delta}=0, \quad \text{and} \quad c(0,z)=f(z). \tag{13}$$

where $f(z)$ is the functional form of the injection zone. We point out that the partial differential equation (12) as well as its semianalytical solution presented in section 3.2 are applicable to a variety of transport processes ranging from the classical Aris-Taylor problem for mass transport in a pressure-driven channel flow to the Graetz/LeVeque problem [see chap. 3 of *Weigand*, 2004; *Graetz*, 1882] in the convective heat transfer communities.

3.2. Solution via Integral Transform

Fully analytical solutions of the advection-dispersion (or convection-diffusion) equation are in general available for uniform coefficients or velocity fields with specific functional forms (e.g., parabolic velocity profile) [e.g., *Özişik and Mikhailov*, 1994; *Weigand*, 2004; *Zoppou and Knight*, 1999]. For a review of different techniques used to solve the advection-dispersion equation with variable coefficients, we refer the interested reader to *de Barros and Cotta* [2007] and references therein. Most (semi)analytical solutions of heat and mass transfer in coupled (porous) matrix/free (laminar) flow systems routinely neglect advective/dispersive transport in the matrix [*Cotta et al.*, 2003; *Roubinet et al.*, 2012; *Martínez et al.*, 2014]. As a result, these models are not representative of transport dynamics above hyperporous matrices (e.g., vegetation) where dispersive mass transport in the obstruction cannot be ignored. The analytical dependence of vertical dispersion on porous matrix permeability is available only for laminar flows in channel/matrix coupled systems [*Ling et al*., 2016].

Studies involving direct numerical simulations of turbulent flows over permeable layers have mainly focused on correlating turbulent structures to obstruction permeability and roughness by combining turbulent closure schemes (e.g., $k-\epsilon$ model) with averaged Darcy-Brinkman-Forchheimer type of models for flow in the obstruction [e.g., *Breugem et al*., 2006; *Suga et al*., 2010, just to mention a few]. Direct numerical simulations of turbulent flows over obstructions, where the pore-scale velocity between obstacles is fully resolved are still computationally prohibitive. Despite its ubiquity to a number of both environmental and technological systems, to the best of our knowledge, theoretical (both analytical and computational) modeling of mass transport in turbulent flows above obstructions has not been fully characterized yet. Existing works are limited to experimental studies and empirical relations which attempt to capture the main transport features [*Ghisalberti and Nepf*, 2005; *Luhar et al*., 2008; *Tanino and Nepf*, 2008; *Nepf*, 2012].

Currently no analytical/semianalytical solution is available to model mass transport in turbulent flows above obstructions (i.e., vegetation) with spatially varying velocity profiles both within and outside the obstruction. Here we employ a modification of the *Generalized Integral Transform Technique* [*Cotta*, 1993; *Özişik and Mikhailov*, 1994] to find a semianalytical solution to (12) and (13) where $u(z)$ is given by (9). The approach has been successfully used to model nonvegetated river flows with nonuniform velocity fields with different functional forms (e.g., parabolic and power law velocity fields) [*de Barros et al*., 2006; *de Barros and Cotta*, 2007]. We refer to *Cotta* [1993], *Özişik and Mikhailov* [1994], and *Özişik* [1993] for theoretical and computational details of the method and its origins.

Let us denote the transformed concentration field by $\bar{c}$. The integral transform and its inverse are defined as follows:

$$\bar{c}_m(y)=\int_0^{1+\delta}\frac{\psi(z;m)}{\sqrt{\mathcal{N}_m}}c(y,z)\mathrm{d}z, \tag{14a}$$

$$c(y,z)=\sum_{m=0}^{\infty}\frac{\psi(z;m)}{\sqrt{\mathcal{N}_m}}\bar{c}_m(y) \tag{14b}$$

respectively, where the norm, $\mathcal{N}_m$, is

$$\mathcal{N}_m=\int_0^{1+\delta}\psi(z;m)^2\mathrm{d}z, \tag{15}$$

and $\psi(z;m)$ corresponds to the eigenfunction basis satisfying the auxiliary Sturm-Liouville problem

$$\frac{\mathrm{d}^2\psi(z;m)}{\mathrm{d}z^2}+\beta_m^2\psi(z;m)=0 \tag{16}$$

subject to

$$\frac{\mathrm{d}\psi(z;m)}{\mathrm{d}z}\Big|_{z=0}=0 \quad \text{and} \quad \frac{\mathrm{d}\psi(z;m)}{\mathrm{d}z}\Big|_{z=1+\delta}=0. \tag{17}$$

The solution of (16) and (17) for the eigenfunctions $\psi(z;m)$ and the eigenvalues β_m is

$$\psi(z;m)=\cos(\beta_m z), \tag{18a}$$

$$\beta_m=\frac{m\pi}{1+\delta}. \tag{18b}$$

Given (18),

$$\mathcal{N}_m:=\frac{1+\delta}{2} \quad \text{for any} \quad m=\{1,2,\dots\} \quad \text{and} \quad \mathcal{N}_0:=1+\delta. \tag{19}$$

The selection of the homogeneous auxiliary problem to determine the eigenfunctions $\psi(z;m)$ is nonunique [*Özişik and Mikhailov*, 1994; *Cotta*, 1993]. Here we choose the auxiliary problem (16) with eigenfunction basis (18) to expand $c(y, z)$, since the convergence rate of (14b) is deemed appropriate. Alternative auxiliary problems (that may include information regarding the spatially variable coefficients of (12)) can be employed to improve the convergence rate [e.g., *Guerrero and Skaggs*, 2010]. Such alternative formulations for the Sturm-Liouville problem can be found in *Cotta* [1993] and *Özişik and Mikhailov* [1994].

We operate (12) and (13) with the integral transform (14a) to obtain

$$\int_0^{1+\delta} \psi(z;m)u(z)\frac{\partial c(y,z)}{\partial y}\mathrm{d}z = \int_0^{1+\delta} \psi(z;m)\frac{\partial}{\partial z}\left[D_v(z)\frac{\partial c(y,z)}{\partial z}\right]\mathrm{d}z. \tag{20}$$

Inserting (14b) in (20), while accounting for (17), leads to the following system of coupled ordinary differential equations (ODEs) (for details, see Appendix A)

$$\sum_{j=0}^{\infty} \mathcal{A}_{mj}\frac{\mathrm{d}\bar{c}_j(y)}{\mathrm{d}y} = \sum_{j=0}^{\infty} \mathcal{B}_{mj}\bar{c}_j(y), \tag{21}$$

subject to

$$\bar{c}_m(0) = \int_0^{1+\delta} \frac{\psi(z;m)}{\sqrt{\mathcal{N}_m}}c(0,z)dz = \int_0^{1+\delta} \frac{\psi(z;m)}{\sqrt{\mathcal{N}_m}}f(z)dz \equiv \bar{f}_m \tag{22}$$

with

$$\mathcal{A}_{mj} = \int_0^{1+\delta} \psi(z;m)\psi(z;j)u(z)\mathrm{d}z, \tag{23a}$$

$$\mathcal{B}_{mj} = \int_0^{1+\delta} \psi(z;j)\frac{\partial}{\partial z}\left[D_v(z)\frac{\partial}{\partial z}\psi(z;m)\right]\mathrm{d}z, \tag{23b}$$

where $u(z)$ and $\psi(z;m)$ are defined by (9) and (18), respectively. Given the functional form of $u(z)$ and $D_v(z)$, and the fact that $\psi(z;m)$ is a trigonometric function, see equation (18a), the integrations involved in both $\mathcal{A}_{mj}$ and $\mathcal{B}_{mj}$ can be analytically calculated (see Appendix B). However, depending on the functional form of the velocity and diffusivity profiles, numerical quadratures can be employed to determine $\mathcal{A}_{mj}$ and $\mathcal{B}_{mj}$. The system of ODEs (21) can be computed using any readily available numerical solver. Note that for a point injection at $(y, z) = (0, z_o)$, (22) reduces to $\psi(z_o;m)/\sqrt{\mathcal{N}_m}$.

The functions $\bar{c}_m(y)$, with $m = 0, \ldots, \infty$, are determined as the solution of the coupled ODE system (21) subject to (22). Finally, the concentration $c(y, z)$ is obtained by truncating the series expansion (14b), e.g., $m = (0, \ldots, M_{\max})$. The choice of the truncation order M_{max} in (14b) is based on the convergence rate of the concentration field. For the upcoming computational examples, we achieved a good convergence with a truncation order of $M_{max} = 50$ in (14b). The dimensionless concentration converged to three significant digits for downstream locations near the source and four significant digits at location far from the injection zone. For multidimensional problems, the convergence rate can be improved if an eigenvalue reordering technique is used [e.g., *Correa et al.*, 1997; *de Barros and Cotta*, 2007].

Given that the system of ODEs is coupled, see equation (21), a closed-form solution for $\bar{c}_m(y)$ is not available. Nonetheless, an approximate solution for $\bar{c}_m(y)$ can be derived by considering only the diagonal elements of $\mathcal{A}_{mj}$ and $\mathcal{B}_{mj}$ in the solution. By setting $m = j$, the system of ODEs becomes decoupled,

$$\mathcal{A}_{mm}\frac{\mathrm{d}\bar{c}_m(y)}{\mathrm{d}y} = \mathcal{B}_{mm}\bar{c}_m(y), \tag{24}$$

subject to $\bar{c}_m(0) = \bar{f}_m$, see (22). The solution of the decoupled system of ODEs is

$$\bar{c}_m(y) = \bar{f}_m \exp\left[\frac{\mathcal{B}_{mm}}{\mathcal{A}_{mm}}y\right]. \tag{25}$$

Substituting (25) in (14b), we obtain the following approximate solution for the concentration field,

$$c(y,z) = \left[\frac{1}{1+\delta}\int_0^{1+\delta} f(z)dz\right] + \sum_{m=1}^{\infty}\frac{\psi(z;m)\bar{f}_m}{\sqrt{\mathcal{N}_m}}\exp\left[\frac{\mathcal{B}_{mm}}{\mathcal{A}_{mm}}y\right], \tag{26}$$

where the first term represents the spatial average of the boundary condition at $y = 0$, see equation (13). The solution (26) is also known as the lowest-order solution [*Cotta and Özişik*, 1986].

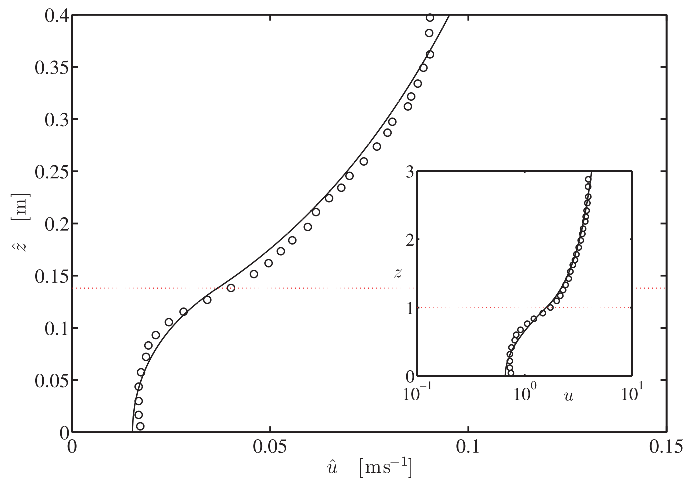

Figure 2. Mean velocity field $\hat{u}(\hat{z})$ measured (empty circles) [*Ghisalberti and Nepf*, 2005, Run I] and predicted (solid line) for $\lambda=1.90$ [*Battiato and Rubol*, 2014]. The inset shows a plot of $u(z)$ (solid line) and the appropriately rescaled data. Adapted from *Battiato and Rubol* [2014].

We emphasize that the concentration profile (14b) can be fully determined once the canopy layer permeability λ, the dispersion coefficient $D_v(z)$, and the geometrical properties of the channel are specified. In the following section, we compare the prediction of our semianalytical solution with experimental data and investigate the role of permeability in controlling the spreading behavior of the solute cloud.

4. Results and Discussion

4.1. Comparison With Experimental Data

To test the capability of the proposed model, we compare the semianalytical solution (14b) with the experimental data collected by *Ghisalberti and Nepf* [2005]. The experiments were performed in a rectangular flume 0.467 m high ($H+L=0.467$ m) and 0.38 m wide ($B=0.38$ m), with rigid vegetation 0.139 m tall ($H=0.139$ m) planted at the bottom of the channel with a density $a=8$ m^{-1} [*Ghisalberti and Nepf*, 2005]. A conservative tracer is injected at the top of the canopies with twelve needles of 9.0 mm diameter each, and a concentration ranging between 120 and 250 g/L. The data include steady state measurements of the (fully developed) mean velocity profile $u(z)$ and concentration profiles $c(y, z)$ at six selected locations downstream ($y_1=0.19$ m, $y_2=0.54$ m, $y_3=0.92$ m, $y_4=1.5$ m, $y_5=2.5$ m, $y_6=3.8$ m) for run I [*Ghisalberti and Nepf*, 2005, Table 1]. A sketch of the experimental setup along with the experimental conditions is shown in Figure 1 and Table 1 of *Ghisalberti and Nepf* [2005].

In the following, we present the calibration and validation procedure which entails two steps: (i) estimation of canopy layer effective permeability K (or equivalently λ) for the calculation of the mean velocity profile and (ii) estimation of the dispersion coefficient D_v.

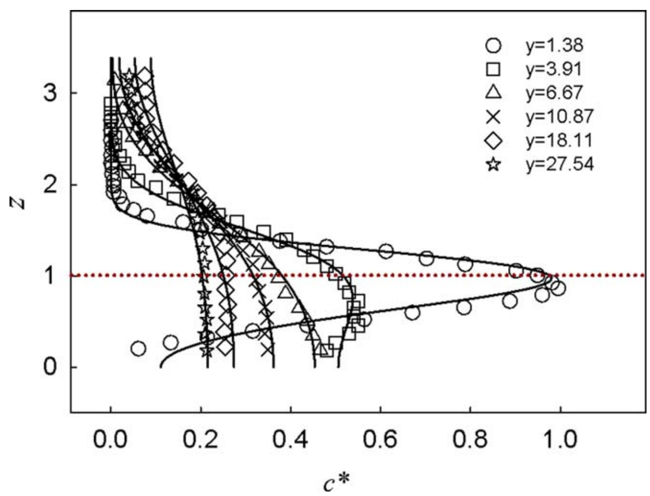

Figure 3. Semianalytical predictions of the concentration profiles at selected locations superimposed to the data of *Ghisalberti and Nepf* [2005]. The dimensionless concentration $c^*(y,z)$ is defined as the dimensional concentration $\hat{c}$ normalized by the maximum concentration measured at $\hat{y}_1=0.19$ m (or $y_1=1.38$) and $\hat{z}=H$ (or $z=1$). The following values of D_v have been employed in the simulations: $D_v=1.9$ cm^2/s at $\hat{y}_1=0.19$ m, $D_v=3.0$ cm^2/s at $\hat{y}_2=0.54$ m, and $D_v=4.5$ cm^2/s for the remaining sections.

4.1.1. Flow Model Calibration and Validation

While a complete discussion on estimating canopy layer permeability can be found in [*Battiato and Rubol*, 2014, section 3], for completeness we provide an outline of the procedure here. The inverse of the dimensionless permeability, λ, can be estimated by a one-point fit of the interfacial velocity, $u(z=1)$. The fitted λ value is then used to infer the full velocity profile for other values of z, other operating flow conditions and/or channel slopes. An alternative approach to estimate permeability is to employ geometrical features of the stem arrangement, such as mean leaf area index (LAI), canopy layer porosity, etc. A discussion on the functional relationship between permeability and canopy topology for ordered arrays of cylinders is given in *Battiato and Rubol* [2014, equation (35), p. 10]. Extensions to random arrays and more realistic canopy configurations is subject of current investigations. Permeability calibration for run I leads to $\lambda=1.90$. Figure 2 shows a comparison between the velocity data collected by *Ghisalberti and Nepf* [2004] and the predicted velocity profile (9) for run I [*Battiato and Rubol*, 2014]. We refer to *Battiato and Rubol* [2014, section 3] for a detailed discussion and additional details on the flow model validation.

4.1.2. Transport Model Calibration and Validation

Once λ and $u(z)$ are determined, an estimate of the dispersion coefficient D_v is required to compute $c(y, z)$ in equation (14b). This is achieved by fitting (14b) with experimental concentration profiles. Validation of the transport model is conducted by comparing the predicted concentration profile with an independent set of data (e.g., concentration at different locations downstream of the injection point) on the same canopy system.

Notwithstanding the model's capability to explicitly account for a spatially dependent D_v (e.g., decreasing eddy diffusivity in proximity of the riverbed), here we show that fitting a constant value of D_v is sufficiently accurate in reproducing the experimental concentration profiles through and over the vegetated layer for dense canopies measured by *Ghisalberti and Nepf* [2005]. Figure 3 shows the comparison between the fitted semianalytical model and the concentration data at six selected locations downstream of the injection point. The model is able to capture the asymmetry of the concentrations profiles, as well as the decrease of the concentration peak with increasing distance from the source. The fitted D_v increases from 1.9 cm^2/s close to the injection point (i.e., y_1) to a constant value of 4.5 cm^2/s for the remaining sections, located downstream ($y \geq y_3$), where the dispersion coefficient is expected to be constant [*Fischer*, 1979] (see details in the caption of Figure 3). Once the dispersion coefficient reaches a constant value, the concentration profiles located at sections further downstream can be predicted by our model without any fitting. In the current analysis, we predicted the concentration profiles at positions $y > y_3$ where D_v reached its constant value. Noticeably, D_v in the far field is in perfect agreement with the one measured by *Ghisalberti and Nepf* [2005] for the same data set, which provides validation of the calibrated model. The fitted D_v value in the far field corresponds to $Sc_t \approx 0.6$ and is in good agreement with available estimates of the turbulent Schmidt number for vegetated flow. Based on experimental data, several works [e.g., *Ghisalberti and Nepf*, 2005, and references therein] report the ratio between mass and momentum transfer to be less than unity for vegetated flows, generally $Sc_t \approx 0.5$ for transport in vegetated flows. Since the Sc_t is defined as the ratio between the eddy kinematic viscosity $\nu_T=\mu_T/\rho$, with μ_T given by (7), and the diffusivity D_v, a comparative estimate of the diffusivity D_v can be obtained from $D_v=\nu_T/Sc_t$.

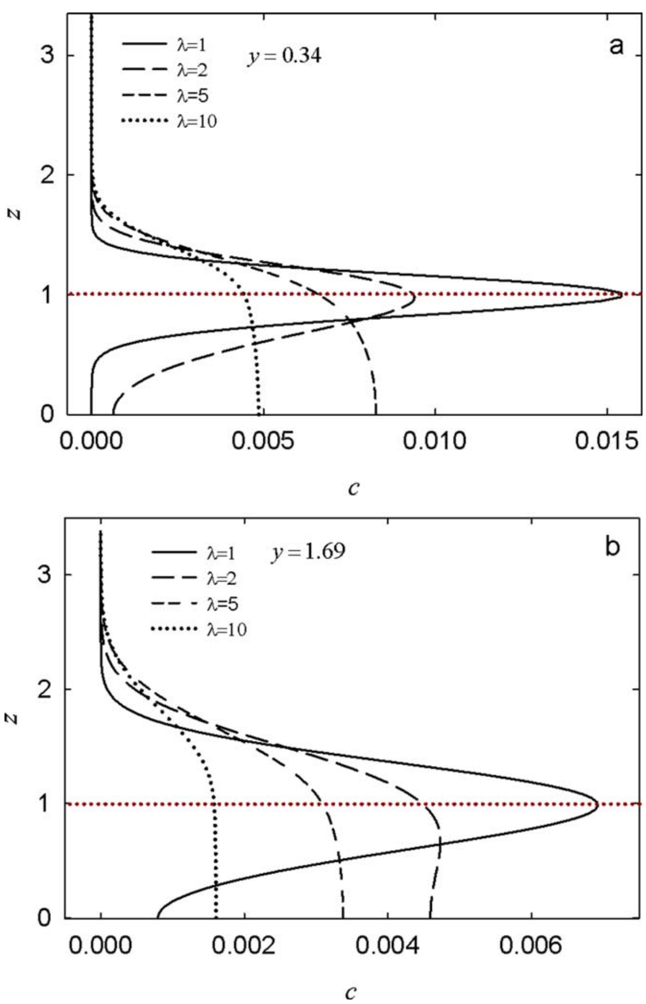

Figure 4. Vertical concentration profile for different canopy permeability values (a) close and (b) far from the injection source. Increasing values of λ indicate denser vegetation, i.e., less permeable canopies.

4.2. Effect of Canopy Geometry

Next, we investigate the effect of canopy geometry on the concentration profile. In the analysis that follows, the solute is injected at the canopy height. As displayed in Figure 4, the asymmetry of the concentration profile increases as the permeability of the vegetation layer decreases. This effect is noticeable when comparing results between less dense (i.e., more permeable) and more dense canopies ($\lambda=1$ and $\lambda=10$, respectively). This is in agreement with the experimental observations of transport over rigid canopies where the asymmetry in the concentration profile increases with the canopy density [*Ghisalberti and Nepf*, 2005; *Nepf and Ghisalberti*, 2008]. The strong velocity shear at the interface of the canopy leads to an increase in vertical mass transfer (Figure 4). It is worth noticing that the decrease in the concentration peak as a result of either distance from the source (Figure 3) or increased canopy density (Figure 4) is due to mechanical dispersion. The mechanism that controls dispersion is the mass flux between the canopy and the free flow [*Ling et al.*, 2016]. Interfacial mass flux is enhanced by concentration differentials across the interface and controlled either by the canopy density (which regulates the shear stress at the interface) or by the distance from the injection point. As a result, plume dispersion is enhanced with increasing the distance from the source or the canopy density. As observed in both Figures 4a and 4b, the permeability of the canopy has a significant role in deviating the concentration profile from the typical Gaussian shape. For locations close to the solute source ($y=0.34$), Figure 4a shows that the solute reaches the riverbed for $\lambda>2$. Furthermore, the peak concentration is approximately reduced by 40% as λ changes from $\lambda=1$ to $\lambda=2$ (see Figure 4a). Figure 4b shows the concentration profile further downstream from the injection zone $y=1.69$. The concentration profiles depicted in Figure 4b illustrate that the distribution of solute inside the canopy layer is quite uniform for $\lambda>1$. This implies that the concentration profiles become more uniform as the Darcy number (D_a) decreases, see equation (8).

To further explore the flexibility of the semianalytical features of the integral transform solution, we investigate the effect of canopy morphology on the vertical dispersion of the solute cloud. The vertical spreading behavior is computed through the second central spatial moment, σ, of the solute cloud:

$$\sigma(y)=\mu_2(y)-[\mu_1(y)]^2, \tag{27}$$

where

$$\mu_2(y)=\frac{1}{\mu_o(y)}\int_0^{1+\delta} z^2 c(y,z)\mathrm{d}z, \tag{28a}$$

$$\mu_1(y)=\frac{1}{\mu_o(y)}\int_0^{1+\delta} zc(y,z)\mathrm{d}z, \tag{28b}$$

$$\mu_0(y)=\int_0^{1+\delta} c(y,z)\mathrm{d}z, \tag{28c}$$

with μ_0 denoting the total resident mass at y integrated over the river depth. Substituting (14b) in (27) and integrating over z leads to

$$\mu_2(y)=\frac{(1+\delta)^{5/2}}{\mu_0(y)}\left[\frac{1}{3}\bar{c}_0(y)+\frac{2\sqrt{2}}{\pi^2}\sum_{m=1}^{\infty}\frac{(-1)^m}{m^2}\bar{c}_m(y)\right], \tag{29}$$

$$\mu_1(y)=\frac{(1+\delta)^{3/2}}{\mu_0(y)}\left\{\frac{1}{\sqrt{2}}\bar{c}_0(y)+\frac{1}{\pi^2}\sum_{m=1}^{\infty}\left[\frac{(-1)^m-1}{m^2}\right]\bar{c}_m(y)\right\}, \tag{30}$$

$$\mu_0(y)=\bar{c}_0(y)\sqrt{(1+\delta)}, \tag{31}$$

since $\sin(m\pi)/m\pi \to 1$ as $m\to 0$, and $\cos(m\pi)=(-1)^m$.

Figure 5 shows the longitudinal evolution of the second central moment (σ) of the solute cloud for different values of λ. These results show the significance of the canopy permeability in controlling the vertical growth rate of solute cloud until it reaches its asymptotic value. For low permeable vegetation structures (i.e., larger λ) corresponding to denser canopies, the velocity shear between the canopy layer and the free layer is large [e.g., *Ghisalberti and Nepf*, 2005; *Battiato and Rubol*, 2014]. As observed in Figure 5 (see curve for $\lambda=10$), this large velocity shear augments vertical mass transfer and as a consequence, mixing along

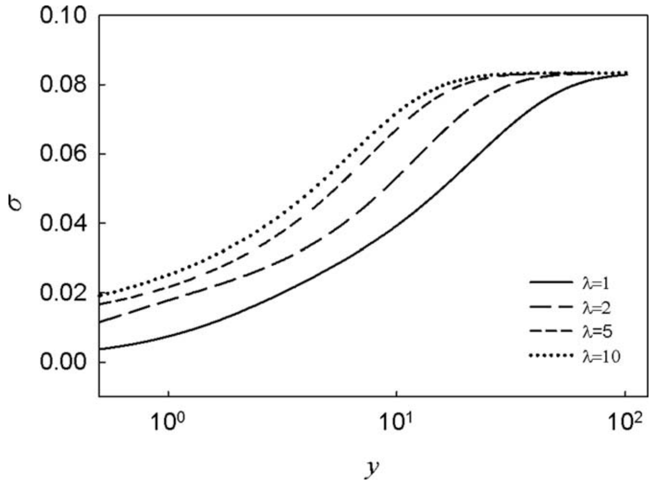

Figure 5. Vertical second central spatial moment σ of the solute cloud for different value of λ as a function of dimensionless longitudinal distance y. Increasing values of λ indicate denser vegetation, i.e., less permeable canopies.

the river depth becomes more efficient. On the contrary, the vertical growth rate of the cloud's spatial moment is slower for $\lambda = 1$ (e.g., more permeable canopy layer) when compared to the case of $\lambda = 10$ (Figure 5). The spatial moment analysis highlights the importance of considering the canopy permeability in predictive models. This is particularly important because canopy permeability exerts a critical control in vertical mixing rates which has implication in nutrient delivery in the riverbed and consequently, the hyporheic zone [*Tonina and Buffington*, 2009].

Next, we investigate the effect of canopy permeability in reducing the peak concentration of the solute cloud. The computation of the peak concentration is important in many applications since it provides information related to (i) the corresponding risks to human health and the environment [*Tartakovsky*, 2013; *de Barros and Fiori*, 2014] and (ii) the dilution potential of the hydrological system [*Fiori*, 2001; *de Barros et al*., 2015]. Figure 6 depicts the maximum concentration observed along the river depth at a fixed longitudinal position downstream from the injection zone as a function of λ. The maximum concentration (c_{max}) is evaluated as follows:

$$c_{\max}(y) = \max_{z \in [0, 1+\delta]} c(y, z). \tag{32}$$

As shown in Figure 6, the maximum concentration reduces with increasing λ. As the permeability of the canopy layer decreases, a higher shear is generated in the velocity profile which augments vertical mass transfer and therefore, the distribution of the concentration field. The results displayed in Figure 6 highlight the role of the canopy in attenuating the peak concentration.

Finally, we compare the results from the semianalytical solution with the fully analytical approximate (lowest-order) solution (26). The longitudinal concentration profiles are computed at $z = 0.68$ (below canopy height) and $z = 1$ (at canopy height) and are displayed in Figures 7a and 7b. As expected, the concentration decreases with y at $z = 1$ (location where the tracer is continuously injected), see Figure 7a. Below the canopy height, Figure 7b shows that the concentration starts to increase and then reduces with y. Results displayed in Figure 7 are reported for $\lambda = 1$ and $\lambda = 2$. As shown in Figure 7, the approximate solution (solid lines) captures the overall behavior of the concentration profile reasonably well. At the canopy height ($z = 1$), the approximate solution (26) overestimates the concentration values (see Figure 7b). Physically, this implies that mixing is underestimated with the lowest-order

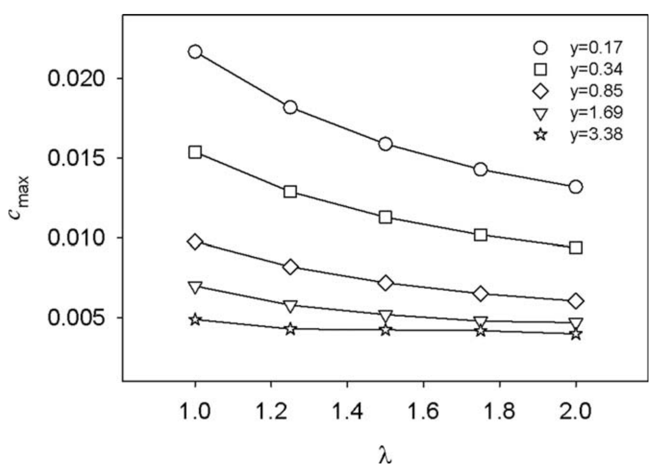

Figure 6. Peak concentration versus λ. Results obtained at different positions downstream of the source. Increasing values of λ indicate denser vegetation, i.e., less permeable canopies.

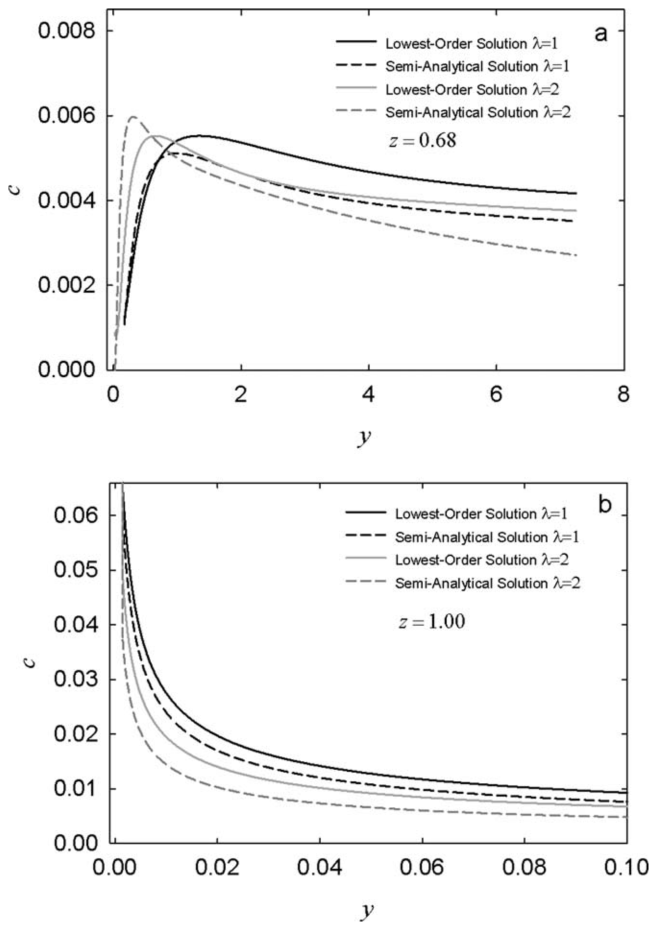

Figure 7. Longitudinal concentration profile obtained using the semianalytical solution and the approximate (lowest-order) solution (26). Concentration profiles shown at (a) $z = 0.68$ (below the canopy height) and (b) $z = 1$ (at the canopy height) for different values of λ. Increasing values of λ indicate denser vegetation, i.e., less permeable canopies.

solution. With the exception of y values in the vicinity of the source, similar behavior is observed below the canopy height ($z = 0.68$) in Figure 7a. The performance of the approximate solution deteriorates as λ increases (e.g., the permeability of the canopy decreases). For increasing λ, the off-diagonal terms of $\mathcal{A}_{mj}$ and $\mathcal{B}_{mj}$ start to play a significant role in capturing the effects induced by the strong shear. Nevertheless, our results show that the approximate solution captures the main transport behavior. As shown in Figure 7, the approximate expression presented in equation (26) favors simplicity however it compromises the accuracy in the solution for the concentration field.

5. Summary and Conclusions

Vegetated channels exhibit unique flow and transport features compared to their nonvegetated counterparts, including reduction of near-bed turbulent stresses, increase in riverbank stability and nutrients retention, and control of solute transfer between the free and the canopy flow, just to mention a few. Such mechanisms are controlled by the canopy structure, as demonstrated in a number of experimental studies. Under the assumption that the vegetation layer can be represented as a porous medium, fully characterized by its effective properties (i.e., porosity and permeability), we propose a modeling framework to investigate the impact of vegetation on solute transport in an open channel. Starting from the two-domain approach to model flow over a vegetated layer introduced by *Battiato and Rubol* [2014], we define an advection-dispersion equation (ADE) to model steady state solute transport in a vegetated channel under fully developed turbulent flow. By means of the *Generalized Integral Transform Technique* [*Cotta*, 1993], we obtain a semianalytical solution for the concentration field in terms of the canopy layer effective properties. The derived semianalytical solution is computationally efficient and free of discretization errors associated with numerical methods. Our results indicate that the canopy layer has a major role in controlling solute transport, including the asymmetry of the concentration profile, the magnitude of the peak concentration and the vertical dispersion growth rates of the solute cloud. The model predictions are in good agreement with the experimental data collected by *Ghisalberti and Nepf* [2005]. The analysis indicates the potential of combining the reduced model with integral transform solutions to predict solute transport. Extensions to reactive transport and flexible canopies are subject of current investigations.

Appendix A: Integral Transform Method

Inserting the inverse formula (14b) in advective term of (20) leads to

$$
\begin{aligned}
I_{\mathrm{adv}} &= \frac{1}{\sqrt{\mathcal{N}_m}}\int_0^{1+\delta}\psi(z;m)u(z)\frac{\partial}{\partial y}\left\{\sum_{j=0}^{\infty}\frac{\psi(z;j)}{\sqrt{\mathcal{N}_j}}\bar{c}_j(y)\right\}dz \\
&= \sum_{j=0}^{\infty}\frac{d\bar{c}_j(y)}{dy}\frac{1}{\sqrt{\mathcal{N}_m\mathcal{N}_j}}\int_0^{1+\delta}u(z)\psi(z;m)\psi(z;j)dz \\
&= \sum_{j=0}^{\infty}\frac{\mathcal{A}_{mj}}{\sqrt{\mathcal{N}_m\mathcal{N}_j}}\frac{d\bar{c}_j(y)}{dy}
\end{aligned}
\tag{A1}
$$

where $\mathcal{A}_{mj}$ is defined in (23a). Similarly, inserting (14b) in the diffusive term of equation (20) gives

$$
\begin{aligned}
I_{\mathrm{diff}} &= \int_0^{1+\delta}\frac{\psi(z;m)}{\sqrt{\mathcal{N}_m}}\frac{\partial}{\partial z}\left[D_v(z)\sum_{j=0}^{\infty}\frac{\bar{c}_j(y)}{\sqrt{\mathcal{N}_j}}\frac{\partial\psi(z,j)}{\partial z}\right]dz \\
&= \sum_{j=0}^{\infty}\frac{\bar{c}_j(y)}{\sqrt{\mathcal{N}_m\mathcal{N}_j}}\int_0^{1+\delta}\psi(z;m)\frac{\partial}{\partial z}\left[D_v(z)\frac{\partial\psi(z,j)}{\partial z}\right]dz \\
&= \sum_{j=0}^{\infty}\frac{\mathcal{B}_{mj}}{\sqrt{\mathcal{N}_m\mathcal{N}_j}}\bar{c}_j(y)
\end{aligned}
\tag{A2}
$$

where $\mathcal{B}_{mj}$ is defined by (23b). Additional details can be found in *de Barros and Cotta* [2007]. The coefficients $\mathcal{A}_{mj}$ and $\mathcal{B}_{mj}$ can be determined for any given velocity profile $u(z)$ and dispersion coefficient $D_v(z)$, once the auxiliary problem is chosen. For our work and the velocity profile adopted, we derived full symbolic expressions for $\mathcal{A}_{mj}$ and $\mathcal{B}_{mj}$, reported in Appendix B. In order to gain more flexibility, numerical integrations can be used to evaluate $\mathcal{A}_{mj}$ and $\mathcal{B}_{mj}$.

Appendix B: Symbolic Expressions for the Coefficients $\mathcal{A}_{mj}$ and $\mathcal{B}_{mj}$

Computation of the coefficients $\mathcal{A}_{mj}$ and $\mathcal{B}_{mj}$ can be achieved through numerical and analytical integration techniques. In this appendix, we provide the symbolic expressions for both $\mathcal{A}_{mj}$ and $\mathcal{B}_{mj}$. These symbolic expressions are valid for the velocity profile $u(z)$ defined (9) and a constant $D_v(z)$. They are

$$
\begin{aligned}
\mathcal{A}_{mj} &= \frac{(\delta+1)e^{-\lambda}}{2\lambda^2}\left(\mathcal{F}_{1,mj}+\mathcal{F}_{2,mj}+\mathcal{F}_{3,mj}+\mathcal{F}_{4,mj}\right), \quad z\in(0,1], \\
\mathcal{A}_{mj} &= \frac{\delta+1}{2\pi(i-j)(i+j)}\left(\mathcal{G}_{1,mj}-\mathcal{G}_{2,mj}+\mathcal{G}_{3,mj}\right), \quad z\in(1,1+\delta),
\end{aligned}
\tag{B1}
$$

where

$$
\mathcal{F}_{1,mj} = \frac{C(\delta+1)\left(e^{2\lambda}-1\right)\lambda^3\cos\left[\frac{\pi(m-j)}{\delta+1}\right]}{(\delta+1)^2\lambda^2+\pi^2(m-j)^2}, \tag{B2a}
$$

$$
\mathcal{F}_{2,mj} = \frac{C(\delta+1)\left(e^{2\lambda}-1\right)\lambda^3\cos\left[\frac{\pi(j+m)}{\delta+1}\right]}{(\delta+1)^2\lambda^2+\pi^2(j+m)^2}, \tag{B2b}
$$

$$
\mathcal{F}_{3,mj} = \frac{e^{\lambda}\sin\left[\frac{\pi(m-j)}{\delta+1}\right]\left(2\pi^2C\lambda^2(m-j)^2\cosh(\lambda)+(\delta+1)^2\lambda^2+\pi^2(m-j)^2\right)}{\pi(\delta+1)^2\lambda^2(m-j)+\pi^3(m-j)^3}, \tag{B2c}
$$

$$
\mathcal{F}_{4,mj} = \frac{e^{\lambda}\sin\left[\frac{\pi(j+m)}{\delta+1}\right]\left[2\pi^2C\lambda^2(j+m)^2\cosh(\lambda)+(\delta+1)^2\lambda^2+\pi^2(j+m)^2\right]}{\pi(\delta+1)^2\lambda^2(j+m)+\pi^3(j+m)^3}, \tag{B2d}
$$

with C defined in (10) and

$$
\mathcal{G}_{1,mj} = 2[\delta\ln(\delta+1)+U][m\sin(\pi m)\cos(\pi j)-j\cos(\pi m)\sin(\pi j)], \tag{B3a}
$$

$$
\mathcal{G}_{2,mj} = 2mU\sin\left(\frac{\pi m}{\delta+1}\right)\cos\left(\frac{\pi j}{\delta+1}\right)+2jU\cos\left(\frac{\pi m}{\delta+1}\right)\sin\left(\frac{\pi j}{\delta+1}\right), \tag{B3b}
$$

$$\mathcal{G}_{3,mj}=\delta\left\{(m+j)\mathrm{Si}\left[\frac{(m-j)\pi}{\delta+1}\right]+(m-j)\mathrm{Si}\left[\frac{(m+j)\pi}{\delta+1}\right]+(-m-j)\mathrm{Si}[(m-j)\pi]+(j-m)\mathrm{Si}[(m+j)\pi]\right\}. \tag{B3c}$$

In (B3), Si denotes the sine integral

$$\mathrm{Si}(\zeta)\equiv\int_0^\zeta\frac{\sin(\tau)}{\tau}d\tau. \tag{B4}$$

In the limit of $j\to m$, equation (B1) becomes

$$\begin{aligned}\mathcal{A}_{mm}&=\frac{\mathcal{W}_{mm}(\delta+1)e^{-\lambda}}{2\lambda^2},\quad z\in(0,1],\\ \mathcal{A}_{mm}&=\frac{\mathcal{H}_{mm}}{4\pi m},\quad z\in(1,1+\delta),\end{aligned} \tag{B5}$$

with

$$\begin{aligned}\mathcal{W}_{mm}=&\frac{C\left(e^{2\lambda}-1\right)\lambda}{\delta+1}+\frac{C(\delta+1)\left(e^{2\lambda}-1\right)\lambda^3}{(\delta+1)^2\lambda^2+4\pi^2m^2}\cos\left(\frac{2\pi m}{\delta+1}\right)\\ &+e^{\lambda}\sin\left(\frac{2\pi m}{\delta+1}\right)\frac{\left(8\pi^2C\lambda^2m^2\cosh\lambda+(\delta+1)^2\lambda^2+4\pi^2m^2\right)}{8\pi^3m^3+2\pi(\delta+1)^2\lambda^2m}+\frac{e^{\lambda}}{\delta+1},\\ \mathcal{H}_{mm}=&(\delta+1)\left\{\sin(2\pi m)[\delta\ln(\delta+1)+U]-U\sin\left(\frac{2\pi m}{\delta+1}\right)\right\}-\delta(\delta+1)\left[\mathrm{Si}(2m\pi)-\mathrm{Si}\left(\frac{2m\pi}{\delta+1}\right)\right]\\ &+2\pi\delta m[(\delta+1)\ln(\delta+1)+U-\delta].\end{aligned} \tag{B6}$$

Assuming $D_v(z)=D_v=$ Const, we obtain the following expression

$$\mathcal{B}_{mj}=-\frac{D_v m[j\sin(\pi j)\sin(\pi m)+m\cos(\pi j)\cos(\pi m)-m]}{(j-m)(j+m)}. \tag{B7}$$

Expression (B7) has a singularity when $j\to m$. Solving (B7) in the limit $j\to m$, we get

$$\mathcal{B}_{mm}=-\frac{1}{2}D_v\sin^2(\pi m). \tag{B8}$$

Acknowledgments

I. B. was supported in part by the National Science Foundation under grant 1461608 and the Department of Energy under the Young Investigator Award grant DE-SC0014227. S. R., I. B., and F. de B. were partially supported by the DOE award "A vegetative facies-based multiscale approach to modeling nutrient transport in the Columbia river Basin" (G00011369). Data will be made available upon request. The authors acknowledge the constructive comments made by four anonymous reviewers.

References

Arunachalam, H., S. Onori, and I. Battiato (2015), On veracity of macroscopic lithium-ion battery models, *J. Electrochem. Soc.*, *162*(10), A1940–A1951.

Battiato, I. (2012), Self-similarity in coupled Brinkman/Navier-Stokes flows, *J. Fluid Mech.*, *699*, 94–114.

Battiato, I., and D. M. Tartakovsky (2011), Applicability regimes for macroscopic models of reactive transport in porous media, *J. Contam. Hydrol.*, *120–121*, 18–26.

Battiato, I., and S. Rubol (2014), Single-parameter model of vegetated aquatic flows, *Water Resour. Res.*, *50*, 6358–6369, doi:10.1002/2013WR015065.

Battiato, I., D. M. Tartakovsky, A. M. Tartakovsky, and T. D. Scheibe (2009), On breakdown of macroscopic models of mixing-controlled heterogeneous reactions in porous media, *Adv. Water Resour.*, *32*, 1664–1673.

Boso, F., and I. Battiato (2013), Homogenizability conditions of multicomponent reactive transport processes, *Adv. Water Resour.*, *62*, 254–265.

Breugem, W. P., B. J. Boersma, and R. E. Uittenbogaard (2006), The influence of wall permeability on turbulent channel flow, *J. Fluid Mech.*, *562*, 35–72.

Correa, E., R. Cotta, and H. Orlande (1997), On the reduction of computational costs in eigenfunction expansions of multidimensional diffusion problems, *Int. J. Numer. Methods Heat Fluid Flow*, *7*(7), 675–695.

Costanza, R., et al. (1997), The value of the world's ecosystem services and natural capital, *Nature*, *387*, 253–260.

Cotta, R. M. (1993), *Integral Transforms in Computational Heat and Fluid Flow*, CRC Press, Boca Raton, Fla.

Cotta, R., and M. Özişik (1986), Laminar forced convection inside ducts with periodic variation of inlet temperature, *Int. J. Heat Mass Transfer*, *29*(10), 1495–1501.

Cotta, R., M. Ungs, and M. Mikhailov (2003), Contaminant transport in finite fractured porous medium: Integral transforms and lumped-differential formulations, *Ann. Nucl. Energy*, *30*(3), 261–285.

Cotta, R. M., D. C. Knupp, C. P. Naveira-Cotta, L. A. Sphaier, and J. N. Quaresma (2013), Unified integral transforms algorithm for solving multidimensional nonlinear convection-diffusion problems, *Numer. Heat Transfer Part A*, *63*(11), 840–866.

de Barros, F. P. J., and R. M. Cotta (2007), Integral transforms for three-dimensional steady turbulent dispersion in rivers and channels, *Appl. Math. Modell.*, *31*(12), 2719–2732.

de Barros, F. P. J., and A. Fiori (2014), First-order based cumulative distribution function for solute concentration in heterogeneous aquifers: Theoretical analysis and implications for human health risk assessment, *Water Resour. Res.*, *50*, 4018–4037, doi:10.1002/2013WR015024.

de Barros, F. P. J., W. B. Mills, and R. M. Cotta (2006), Integral transform solution of a two-dimensional model for contaminant dispersion in rivers and channels with spatially variable coefficients, *Environ. Modell. Software*, *21*(5), 699–709.

de Barros, F. P. J., A. Fiori, F. Boso, and A. Bellin (2015), A theoretical framework for modeling dilution enhancement of non-reactive solutes in heterogeneous porous media, *J. Contam. Hydrol.*, *175*, 72–83.

Fiori, A. (2001), The Lagrangian concentration approach for determining dilution in aquifer transport: Theoretical analysis and comparison with field experiments, *Water Resour. Res.*, *37*(12), 3105–3114.

Fischer, H. B. (1979), *Mixing in Inland and Coastal Waters*, Academic, N. Y.

Ghisalberti, M., and H. M. Nepf (2002), Mixing layers and coherent structures in vegetated aquatic flows, *J. Geophys. Res.*, *107*(C2), 3011, doi:10.1029/2001JC000871.

Ghisalberti, M., and H. M. Nepf (2004), The limited growth of vegetated shear layers, *Water Resour. Res.*, *40*, W07502, doi:10.1029/2003WR002776.

Ghisalberti, M., and H. Nepf (2005), Mass transport in vegetated shear flows, *Environ. Fluid Mech.*, *5*(6), 527–551.

Graetz, L. (1882), Ueber die wärmeleitungsfähigkeit von flüssigkeiten, *Ann. Phys.*, *254*(1), 79–94.

Guerrero, J. P., and T. Skaggs (2010), Analytical solution for one-dimensional advection-dispersion transport equation with distance-dependent coefficients, *J. Hydrol.*, *390*(1), 57–65.

Hirata, S., B. Goyeau, D. Gobin, M. Chandesris, and D. Jamet (2009), Stability of natural convection in superposed fluid and porous layers: Equivalence of the one-and two-domain approaches, *Int. J. Heat Mass Transfer*, *52*(1), 533–536.

Kang, H., and S.-U. Choi (2009), Turbulence modeling of solute transport in open-channel flows over submerged vegetation, in *Advances in Water Resources and Hydraulic Engineering*, edited by C. Zhang and H. Tang, pp. 674–679, Springer, Berlin.

Katul, G., D. Poggi, and L. Ridolfi (2011), A flow resistance model for assessing the impact of vegetation on flood routing mechanics, *Water Resour. Res.*, *47*, W08533, doi:10.1029/2010WR010278.

Konings, A., G. Katul, and S. Thompson (2012), A phenomenological model for the flow resistance over submerged vegetation, *Water Resour. Res.*, *48*, W02522, doi:10.1029/2011WR011000.

Kubrak, E., J. Kubrak, and M. R. Rowinski (2008), Vertical velocity distributions through and above submerged, flexible vegetation, *Hydrol. Sci. J.*, *53*(4), 37–41.

Ling, B., A. M. Tartakovsky, and I. Battiato (2016), Dispersion controlled by permeable surfaces: Surface properties and scaling, *J. Fluid Mech.*, *801*, 13–42.

Lowe, R. J., J. R. Koseff, and S. G. Monismith (2005), Oscillatory flow through submerged canopies: 1. Velocity structure, *J. Geophys. Res.*, *110*, C10016, doi:10.1029/2004JC002788.

Lowe, R. J., U. Shavit, J. L. Falter, J. R. Koseff, and S. G. Monismith (2008), Modeling flow in coral communities with and without waves: A synthesis of porous media and canopy flow approaches, *Limnol. Oceanogr. Methods*, *53*(6), 2668.

Luhar, M., J. Rominger, and H. Nepf (2008), Interaction between flow, transport and vegetation spatial structure, *Environ. Fluid Mech.*, *8*(5–6), 423–439.

Marion, A., M. Zaramella, and A. Bottacin-Busolin (2008), Solute transport in rivers with multiple storage zones: The stir model, *Water Resour. Res.*, *44*, W10406, doi:10.1029/2008WR007037.

Martínez, A. R., D. Roubinet, and D. M. Tartakovsky (2014), Analytical models of heat conduction in fractured rocks, *J. Geophys. Res. Solid Earth*, *119*, 83–98, doi:10.1002/2012JB010016.

McNulty, A., and I. Wood (1984), A new approach to predicting the dispersion of a continuous pollutant source, *J. Hydraul. Res.*, *22*(1), 23–34.

Nepf, H. M. (2012), Flow and Transport in Regions with Aquatic Vegetation, *Annu. Rev. Fluid Mech.*, *44*(1), 123–142.

Nepf, H., and M. Ghisalberti (2008), Flow and transport in channels with submerged vegetation, *Acta Geophys.*, *56*(3), 753–777.

Nokes, R., and I. Wood (1988), Vertical and lateral turbulent dispersion: Some experimental results, *J. Fluid Mech.*, *187*, 373–394.

Özişik, M. N. (1993), *Heat Conduction*, Wiley, N. Y.

Özişik, M. N., and M. D. Mikhailov (1994), *Unified Analysis and Solutions of Heat and Mass Diffusion*, Dover Publ., N. Y.

Papke, A., and I. Battiato (2013), A reduced complexity model for dynamic similarity in obstructed shear flows, *Geophys. Res. Lett.*, *40*, 3888–3892, doi:10.1002/grl.50759.

Poggi, D., C. Krug, and G. Katul (2009), Hydraulic resistance of submerged rigid vegetation derived from first-order closure models, *Water Resour. Res.*, *45*, W10442, doi:10.1029/2008WR007373.

Roubinet, D., J.-R. de Dreuzy, and D. M. Tartakovsky (2012), Semi-analytical solutions for solute transport and exchange in fractured porous media, *Water Resour. Res.*, *48*, W01542, doi:10.1029/2011WR011168.

Sphaier, L., R. Cotta, C. Naveira-Cotta, and J. Quaresma (2011), The unit algorithm for solving one-dimensional convection-diffusion problems via integral transforms, *Int. Commun. Heat Mass Transfer*, *38*(5), 565–571.

Stephan, U., and D. Gutknecht (2002), Hydraulic resistance of submerged flexible vegetation, *J. Hydrol.*, *269*, 27–43.

Suga, K., Y. Matsumura, Y. Ashitaka, S. Tominaga, and M. Kaneda (2010), Effects of wall permeability on turbulence, *Int. J. Heat Fluid Flow*, *31*, 974–984.

Tanino, Y., and H. M. Nepf (2008), Lateral dispersion in random cylinder arrays at high Reynolds number, *J. Fluid Mech.*, *600*, 339–371.

Tartakovsky, D. M. (2013), Assessment and management of risk in subsurface hydrology: A review and perspective, *Adv. Water Resour.*, *51*, 247–260.

Thomas, F. I. M., C. D. Cornelisen, and J. M. Zande (2000), Effects of water velocity and canopy morphology on ammonium uptake by seagrass communities, *Ecology*, *81*(10), 2704–2713.

Tonina, D., and J. M. Buffington (2009), Hyporheic exchange in mountain rivers. i: Mechanics and environmental effects, *Geogr. Compass.*, *3*(3), 1063–1086.

Variano, E. A., D. T. Ho, V. C. Engel, P. J. Schmieder, and M. C. Reid (2009), Flow and mixing dynamics in a patterned wetland: Kilometer-scale tracer releases in the everglades, *Water Resour. Res.*, *45*, W08422, doi:10.1029/2008WR007216.

Weigand, B. (2004), *Analytical Methods for Heat Transfer and Fluid Flow Problems*, vol. 263, Springer, Berlin.

White, B. L., and H. M. Nepf (2003), Scalar transport in random cylinder arrays at moderate Reynolds number, *J. Fluid Mech.*, *487*, 43–79.

White, B. L., and H. M. Nepf (2007), Shear instability and coherent structures in shallow flow adjacent to a porous layer, *J. Fluid Mech.*, *593*, 1–32.

Yeh, G.-T., and Y.-J. Tsai (1976), Dispersion of water pollutants in a turbulent shear flow, *Water Resour. Res.*, *12*(6), 1265–1270.

Zoppou, C., and J. Knight (1999), Analytical solution of a spatially variable coefficient advection-diffusion equation in up to three dimensions, *Appl. Math. Modell.*, *23*(9), 667–685.